Available online at www.sciencedirect.com
ScienceDirect
Journal of Magnetic Resonance 190 (2008) 60–67
JMR Journal of Magnetic Resonance
www.elsevier.com/locate/jmr

Reaction fields and solvent dependence of the EPR parameters of nitroxides: The microenvironment of spin labels

Derek Marsh *

Max-Planck-Institut für biophysikalische Chemie, Abteilung Spektroskopie, 37077 Göttingen, Germany

Received 30 April 2007; revised 2 October 2007
Available online 16 October 2007

Abstract

The sensitivity of nitroxide spin-label EPR to the polarity of aprotic environments arises from the reaction field produced by polarisation of the surrounding dielectric by the nitroxide electric dipole moment. The performances of three different reaction fields that have been proposed as improvements on the original Onsager model are compared for representative spin-label nitroxides in a range of apolar and dipolar aprotic solvents. Explicit allowance is made for the polarisability of the nitroxide, which effectively renormalises the reaction field but has been neglected in previous analyses of nitroxide hyperfine couplings when using the improved reaction fields. It is found that the model of Block and Walker, which incorporates an exponential dependence of the dielectric permittivity on inverse radial distance from the nitroxide, gives the best description of the solvent dependence of the isotropic ^{14}N-hyperfine couplings. These results should be useful not only for calibration of environmental polarity using homogeneous solvents, but also for transferring polarity scales and polarity profiles (e.g., in membranes) between different nitroxide spin labels (e.g., of the TEMPO and DOXYL variety).

Keywords: Hyperfine coupling; *g*-value; Nitroxide; Spin label; Polarity; Reaction field

1. Introduction

As for other spectroscopies (and, indeed, for solvation in general) [1,2], the spectral line positions in EPR depend on solvent polarity by virtue of the reaction field induced by the electric dipole moment of the free radical of interest. This gives rise to the well-known sensitivity of nitroxide spin-label hyperfine couplings to environmental polarity [3–5], which has important applications in lipid membranes, peptides and proteins (see, e.g., Refs. [6–14]).

Conventionally, analyses of isotropic hyperfine couplings in aprotic solvents have used the Onsager dielectric-continuum model [15] of the reaction field [3,16–19]. With allowance for the polarisability of nitroxide free radicals, the increment in hyperfine coupling is predicted to vary as $(\varepsilon_r - 1)/(\varepsilon_r + 1)$ in the Onsager model, where ε_r is the relative dielectric permittivity of the solvent. However, this functional dependence of the reaction field saturates too rapidly with increasing dielectric permittivity [1,5], and therefore does not describe well the hyperfine couplings in strongly dipolar aprotic solvents (see Refs. [3,20]). The reason for this is that a step-function in dielectric permittivity is assumed for the transition to the dielectric continuum at the molecular surface, and this does not take into account the local interactions.

There have been several attempts to improve upon the basic Onsager model by introducing a more gradual transition in dielectric permittivity. These include an exponential dependence on inverse radial distance [21], a direct exponential dependence on radial distance [22], and a statistical mechanical model for polarisable, dipolar hard-sphere fluids [23,24]. Each of these alternatives to the Onsager model has been applied by one or other authors to analysis of the solvent dependence of nitroxide hyperfine couplings, pioneered in the first instance by Reddoch and Konishi [20]. The Block and Walker reaction field was used by Abe et al. [25], the direct exponential model by Ehrenson [26],

* Fax: +49 551 201 1501.
E-mail address: dmarsh@gwdg.de

1090-7807/$ - see front matter © 2007 Elsevier Inc. All rights reserved.
doi:10.1016/j.jmr.2007.10.004

and the Wertheim model was used by Reddoch and Konishi [20] and by Ottaviani et al. [27]. However, unlike the applications of the Onsager model, the polarisability of the nitroxide was omitted from all these treatments.

In the present work, we compare the performance of all four of the above reaction fields in interpreting the solvent dependence of hyperfine couplings (and, to a lesser extent, g-values), for various representative nitroxide spin labels in a wide range of aprotic media. The polarisability of the nitroxide is included in every case, and is found to have a particularly significant effect for the Wertheim model. An analysis such as this is important not only for comparison of spin-labelled biological environments with solutions of defined polarity, but also for transfer of polarity dependences between different nitroxide spin labels [28,29]. The latter is particularly significant for transmembrane polarity profiles that are established mostly by oxazolidine-nitroxide spin-labelled lipids [30–32], whereas integral membrane peptides and proteins are mostly spin-labelled with piperidine-, pyrrolidine- or pyrroline-nitroxide derivatives (e.g., Refs. [33–35]). Similar considerations apply also to the polarity and/or solvent dependence of chemical shifts in NMR.

2. Reaction field

In the absence of an external field, the total electric dipole moment of a nitroxide immersed in a dielectric is:

$$\mathbf{m} = \mathbf{p} + \alpha \mathbf{E}_R \tag{1}$$

where $\mathbf{p} \sim 10^{-29}$ C.m (3 Debye) is the permanent electric dipole moment of the nitroxide [36,37], α is the polarisability of the nitroxide, and $\mathbf{E}_R$ is the reaction field at the nitroxide that results from polarisation of the dielectric by the dipole moment of the nitroxide. In the Onsager approach, the reaction field may therefore be expressed in the form:

$$\mathbf{E}_R = f(\varepsilon_r)\frac{\mathbf{m}}{4\pi\varepsilon_o r_{eff}^3} \tag{2}$$

where ε_r is the relative dielectric permittivity of the medium, ε_o is the permittivity of free space, and r_{eff} is the effective molecular radius of the nitroxide. Note that with $\mathbf{m} = \mathbf{p}$, Eq. (2) is the reaction field for a non-polarisable dipole. Combining Eqs. (1) and (2), the reaction field is given by [15]:

$$\mathbf{E}_R = \frac{f(\varepsilon_r)}{1 - f(\varepsilon_r)\frac{\alpha}{4\pi\varepsilon_o r_{eff}^3}} \cdot \frac{\mathbf{p}}{4\pi\varepsilon_o r_{eff}^3} \tag{3}$$

Therefore, comparing Eqs. (2) and (3), the dipole moment of the polarisable nitroxide is renormalised by a factor $[1 - f(\varepsilon_r)\alpha/(4\pi\varepsilon_o r_{eff}^3)]^{-1}$ as a result of the reaction field. In the presence of an external field, the polarisability α is renormalised by exactly the same factor, as will be seen later.

The electronic polarisability, α, can be expressed in terms of the refractive index, n_D, of the pure nitroxide by using the Lorenz–Lorentz relation:

$$\frac{n_D^2 - 1}{n_D^2 + 2} = \frac{\alpha}{4\pi\varepsilon_o r_{eff}^3} \tag{4}$$

Hence, the reaction field for a polarisable nitroxide is given by:

$$\mathbf{E}_R = \frac{f(\varepsilon_r)}{1 - f(\varepsilon_r)\frac{n_D^2-1}{n_D^2+2}} \cdot \frac{\mathbf{p}}{4\pi\varepsilon_o r_{eff}^3} \tag{5}$$

which, in contrast to Eq. (2), is expressed in terms of the permanent electric dipole, $\mathbf{p}$, instead of the total dipole, $\mathbf{m}$. The reaction field is parallel to the dipole moment $\mathbf{p}$ and therefore, unlike an external field, does not affect its orientation.

The function $f(\varepsilon_r)$ in Eq. (5) depends on the model assumed for calculating the reaction field in Eq. (2). In the Onsager model for condensed fluids, a spherical molecule of radius r_{eff} is immersed in a homogeneous dielectric of scalar dielectric constant ε. Solution of Laplace's equation then yields [15]:

$$f_o(\varepsilon_r) = \frac{2(\varepsilon_r - 1)}{2\varepsilon_r + 1} \tag{6}$$

This leads to a compact expression for the strength of the reaction field:

$$\mathbf{E}_R(\text{Onsager}) = \frac{2(n_D^2 + 2)(\varepsilon_r - 1)}{3(2\varepsilon_r + n_D^2)} \frac{\mathbf{p}}{4\pi\varepsilon_o r_{eff}^3} \tag{7}$$

where for nitroxides $n_D^2 \approx 2$ (see, e.g., Ref. [20]). The Onsager reaction field is approximately proportional to $(\varepsilon_r - 1)/(\varepsilon_r + 1)$ which, as is well known, saturates too quickly with increasing dielectric constant [5,38] (see Fig. 1). The Onsager

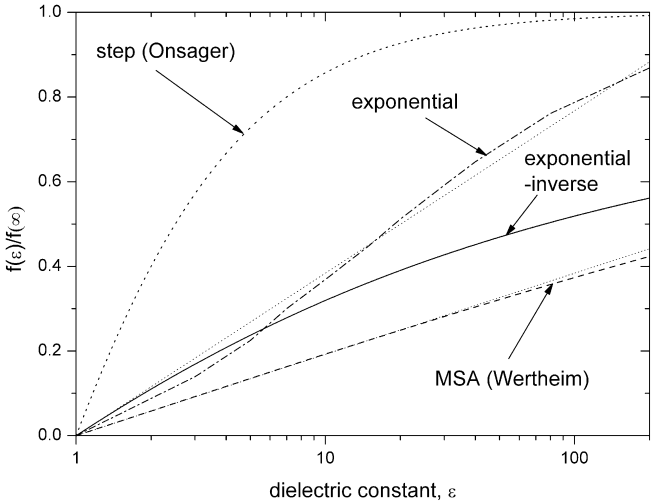

Fig. 1. Dependence of $f(\varepsilon_r)$, which determines the reaction field according to Eq. (2), on bulk dielectric permittivity, ε_r, of the medium. *Heavy dotted line*: Onsager model for a step transition in ε_r [15], Eq. (6), $f_o(\infty) = 1$; *solid line:* exponential-inverse transition in ε_r of Block and Walker [21], Eq. (8), $f_{BW}(\infty) = 1$; *dash and dotted line:* direct exponential transition in ε_r [22], $f_E(\infty) = 1$; *dashed line*: Wertheim model for a polarisable, hard-sphere, dipolar fluid in the mean spherical approximation [23,24], Eqs. (9) and (12), $f_W(\infty) = 8$. *Light dotted, straight lines* are the approximations $f(\varepsilon_r) = \frac{1}{6}\ln\varepsilon_r$ and $f(\varepsilon_r) = \frac{1}{12}\ln\varepsilon_r$, respectively.

model therefore is applicable only to media with low dielectric constants. Alternative reaction fields have been considered by Reddoch and Konishi [20], by Abe et al. [25], by Ehrenson [26] and by Ottaviani et al. [27], when interpreting the dependence of nitroxide hyperfine couplings on solvent dielectric constant.

A possible modification to the Onsager model that was put forward by Block and Walker [21] is to replace the abrupt step to a homogeneous dielectric, at the molecular surface, by an exponential transition that depends inversely on radial distance: $\varepsilon_r(r) = \varepsilon_B \exp(-\kappa/r)$. The boundary conditions that $\varepsilon_r = 1$ at the molecular surface $r = r_{eff}$, and that ε_r attains its bulk value, ε_B, as $r \to \infty$, fix the exponential decay constant and therefore no extra parameters are introduced (see Fig. 2). Solution of the Laplace equation then leads to [21]:

$$f_{BW}(\varepsilon_r) = \frac{3\varepsilon_r \ln \varepsilon_r}{\varepsilon_r \ln \varepsilon_r - \varepsilon_r + 1} - \frac{6}{\ln \varepsilon_r} - 2 \tag{8}$$

This, together with Eq. (5), defines the reaction field in the Block–Walker model, which saturates less readily than does that of the Onsager model (see Fig. 1), in accordance with observation. For $\varepsilon_r \to 1$, $f_{BW}(\varepsilon_r) \approx \frac{1}{6} \ln \varepsilon_r$ and for $\varepsilon_r \to \infty$, $f_{BW}(\varepsilon_r) = 1$ [20].

As pointed out by Ehrenson [22], the exponential-inverse transition of Block and Walker [21] reaches the bulk dielectric constant only at large radial distances. A direct exponential transition: $\varepsilon_r(r) = \varepsilon_B - (\varepsilon_B - 1)2^{-(r-r_{eff})/2r_{eff}}$, which reaches half the bulk value at $r = 3r_{eff}$, is shown for comparison in Fig. 2. Numerical solutions for the reaction field, $f_E(\varepsilon_r)$, in this model have been given by Ehrenson [22] and are presented in Fig. 1. As for the other continuum dielectric models, $f_E(\varepsilon_r) = 1$ for $r \to \infty$. The reaction field for this direct exponential transition in dielectric constant saturates more rapidly than does that for the exponential inverse transition, but less rapidly than in the Onsager model.

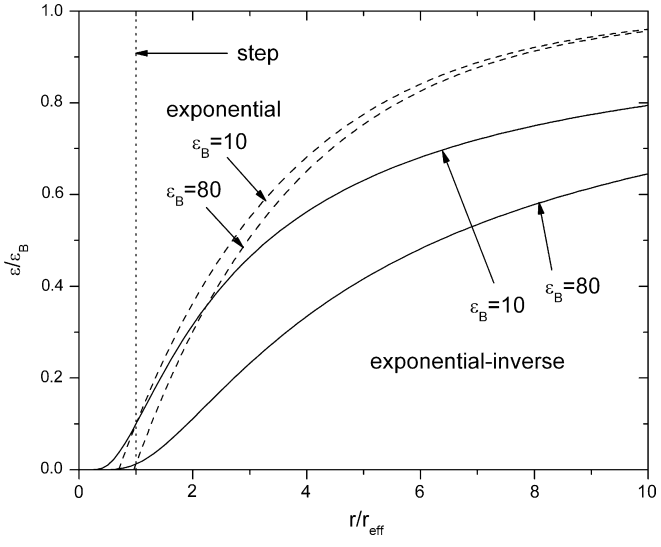

Fig. 2. Radial dependence of the dielectric permittivity for an exponential-inverse transition [21]: $\varepsilon_r = \varepsilon_B \exp(-\ln\varepsilon_B \cdot r_{eff}/r)$ (solid line); or a direct exponential transition [22]: $\varepsilon_r = \varepsilon_B - (\varepsilon_B - 1)2^{-(r-r_{eff})/2r_{eff}}$ (dashed line). Dependences are given for two values of the bulk dielectric permittivity: $\varepsilon_B = 10$ and $\varepsilon_B = 80$, as indicated. The Onsager model (dotted line) assumes a step-function at the molecular surface $r = r_{eff}$.

Wertheim [23] has performed a statistical mechanical calculation for non-polar fluids. A hard-sphere version of the mean spherical approximation (MSA) yields the following parametric result for the dielectric permittivity [23]:

$$\varepsilon_r = \frac{(1+4\xi)^2(1+\xi)^4}{(1-2\xi)^6} \tag{9}$$

The parameter ξ is related to the renormalised polarisability, α', by [23]:

$$\frac{\alpha'}{\alpha} = \left(1 - 16\xi \frac{\alpha}{4\pi\varepsilon_o r_{eff}^3}\right)^{-1} \tag{10}$$

It should be noted that Eqs. (9) and (10) also hold for a polarisable hard-sphere fluid with permanent dipoles, in the mean spherical approximation [24]. In this case, the permanent dipole, **p**, is renormalised by exactly the same factor as is the polarisability (cf. Eqs. (2) and (3)).

In the Onsager approach for an apolar fluid (i.e., $p = 0$), the induced dipole moment is related to α' by the following definition:

$$\mathbf{m} = \alpha(\mathbf{E}_C + \mathbf{E}_R) = \alpha'\mathbf{E}_C \tag{11}$$

where $\mathbf{E}_C$ is the cavity field associated with an external field $\mathbf{E}_o$, and $\mathbf{E}_R$ is the reaction field. In combination with Eq. (2), the renormalised polarisability becomes:

$$\frac{\alpha'}{\alpha} = \left(1 - f_W(\varepsilon_r) \frac{\alpha}{4\pi\varepsilon_o r_{eff}^3}\right)^{-1} \tag{12}$$

Hence, in the mean spherical approximation (MSA) of Wertheim for a polarisable hard-sphere, dipolar fluid [23,24], the function defining the reaction field in Eq. (5) is given from comparing Eqs. (10) and (12) by:

$$f_W(\varepsilon_r) = 16\xi \tag{13}$$

which is related to the dielectric permittivity, ε_r, by Eq. (9) (see also Refs. [39,40]). For $\varepsilon_r = 1$–100, $f_W(\varepsilon_r) \approx \frac{2}{3} \ln \varepsilon_r$ and for $\varepsilon_r \to \infty$, $f_W(\varepsilon_r) = 8$ [20]. Again as seen from Fig. 1, the function $f_W(\varepsilon_r)$ saturates less rapidly than the corresponding Onsager expression. Unlike the continuum dielectric models, however, $f_W(\infty) > 1$ in the Wertheim MSA model. The ensuing much larger values of $f(\varepsilon_r)$ therefore have a very pronounced effect on the polarisability-dependent renormalisation factor $[1 - f(\varepsilon_r)\alpha/(4\pi\varepsilon_o r_{eff}^3)]^{-1}$ in Eq. (3). This is illustrated in Fig. 3 which shows the dependence of the reaction field on dielectric constant predicted from Eq. (5) with $n_D^2 = 2$. The maximum value of $f(\varepsilon_r)/[1 - f(\varepsilon_r)/4]$ is 4/3 for the dielectric continuum models, but for the Wertheim MSA model it already increases steeply at $\varepsilon_r \leqslant 10$. In the Block–Walker model with exponential-inverse transition in ε_r, renormalisation has a relatively small effect for values of ε_r in the region of practical interest.

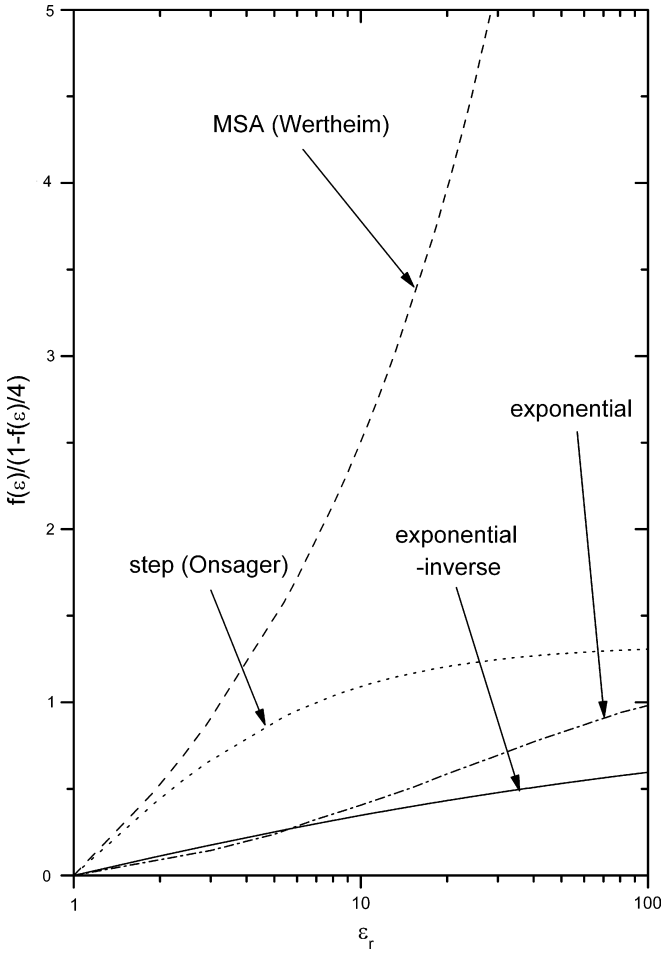

Fig. 3. Dependence of the function $f(\varepsilon_r)/\left(1-\frac{1}{4}f(\varepsilon_r)\right)$, which determines the reaction field according to Eq. (5), on the bulk dielectric permittivity, ε_r, of the medium. *Dotted line:* Onsager model for a step transition in ε [15]; *solid line:* exponential-inverse transition in ε_r [21]; *dash and dotted line*: direct exponential transition in ε_r [22]; *dashed line*: MSA for a polarisable, hard-sphere, dipolar fluid [23,24].

3. Applications

The isotropic ^{14}N-hyperfine coupling, a_o^N, of nitroxide spin labels depends linearly on the unpaired electron spin density on the nitrogen atom [41]. This in turn is perturbed linearly by the local electric field at the nitrogen atom [3,20,25,42]. In terms of the reaction field of Eq. (5), the isotropic hyperfine coupling therefore depends on the dielectric permittivity of the solvent according to:

$$a_o^N = a_o^{\varepsilon=1} + K_v \frac{f(\varepsilon_r)}{1-\frac{1}{4}f(\varepsilon_r)} \qquad (14)$$

where $a_o^{\varepsilon=1}$ is the extrapolated isotropic hyperfine coupling in a medium of relative dielectric permittivity $\varepsilon_r = 1$, and K_v is a constant for a particular nitroxide (see also Ref. [29]). In Eq. (14), it is assumed that $n_D^2 \approx 2$, for the refractive index of the nitroxide.

Structures of the nitroxide spin labels to be considered are given in Fig. 4. Fig. 5 shows the dependence of a_o^N on

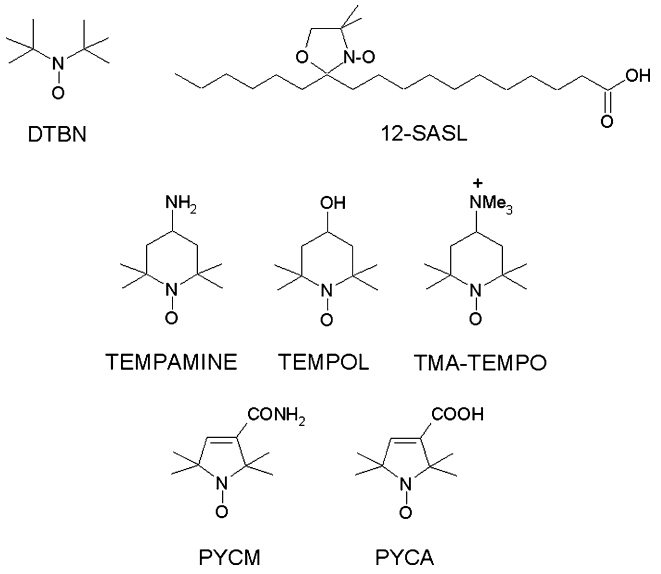

Fig. 4. Structures of spin-label nitroxides: DTBN (di-*tert*-butyl nitroxide); 12-SASL (12-(4,4-dimethyl-oxazolidin-*N*-oxyl)stearic acid); TEMPAMINE, (4-amino-2,2,6,6-tetramethyl-piperidine-1-oxyl); TEMPOL (4-hydroxy-2,2,6,6-tetramethyl-piperidine-1-oxyl); TMA-TEMPO (4-trimethylammonium-2,2,6,6-tetramethyl-piperidine-1-oxyl); PYCM (2,2,5,5-tetramethyl-pyrrolin-1-oxyl-3-carboxamide); PYCA (2,2,5,5-tetramethyl-pyrrolin-1-oxyl-3-carboxylate).

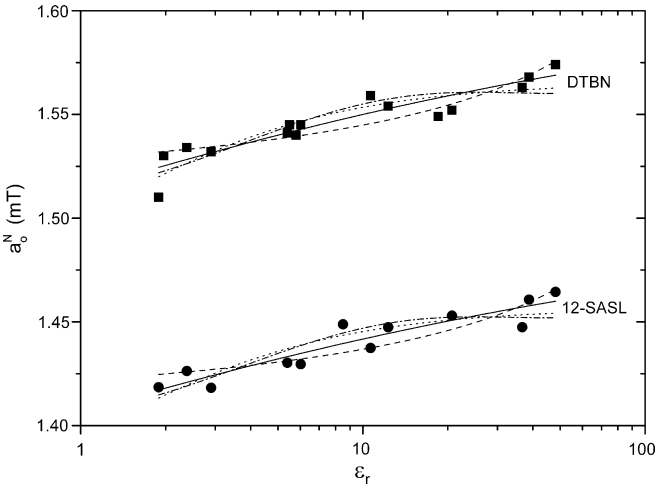

Fig. 5. Dependence of the isotropic hyperfine coupling, a_o^N, on relative dielectric permittivity, ε_r, of the solvent; for DTBN ([3]; squares) and 12-SASL ([29]; circles) nitroxyl spin labels. The data for DTBN are augmented by points for toluene and pyridine from Reddoch and Konishi [20]. Continuous lines are non-linear least-squares fits of the following models: step transition in ε_r ([15]; dotted line); exponential-inverse transition in ε_r ([21]; solid line); direct exponential transition in ε_r ([22]; dash and dotted line); MSA for polarisable, hard-sphere dipoles ([23,24]; dashed line). The abscissa is logarithmic.

relative dielectric permittivity of the solvent for the DTBN [3] and 12-SASL spin labels [29]. All solvents considered are aprotic, i.e., are not functioning as hydrogen-bond donors (cf. Ref. [3]). They consist of both apolar and dipolar solvents, varying from hexane ($\varepsilon_r = 1.89$) to dimethyl sulphoxide ($\varepsilon_r = 48.2$). It is evident from Fig. 5 that the

^{14}N-hyperfine couplings depend approximately linearly on $\ln\varepsilon_r$ for this range of solvents. Non-linear least-squares fits of Eq. (14) to the experimental hyperfine couplings are given with the various models for $f(\varepsilon_r)$ by the different lines in Fig. 5. No model gives a perfect fit, which can be attributed to the existence of additional specific local interactions with the solvent, such as are considered by, e.g., the Kirkwood model of molecular ordering in polar dielectrics [43]. The best overall fit is afforded by the Block–Walker model ($r = 0.93$ for both DTBN and 12-SASL), which is defined by a transition in dielectric permittivity that depends exponentially on the inverse radial distance. For this model, $f_{BW}(\varepsilon_r)/\left(1-\frac{1}{4}f_{BW}(\varepsilon_r)\right)$ approximates most closely to a logarithmic dependence on ε_r. The step-function [15] and direct exponential [22] transitions are characterised by a convex deviation from a logarithmic dependence, whereas the deviations of the Wertheim MSA model for hard-sphere fluids are of the opposite sense, i.e., concave downwards (see Fig. 5).

A feature already noted for the Wertheim MSA model is the steep increase in the function $f_W(\varepsilon_r)/\left(1-\frac{1}{4}f_W(\varepsilon_r)\right)$ for $\varepsilon_r > 10$. Amongst other things, this results in fitted values of K_v being smaller by approximately a factor of 10 for this model than for the other three continuum dielectric models. The fitting parameters for the exponential-inverse Block–Walker model are given in Table 1. For comparison, the values of K_v for 12-SASL that are obtained with the Onsager ($r = 0.89$), direct exponential ($r = 0.89$) and Wertheim models ($r = 0.90$) are: 4.7 ± 0.7, 3.6 ± 0.6 and $0.60 \pm 0.09 \times 10^{-2}$ mT, respectively. Similar values are also obtained for DTBN with these three models, except that the regression coefficient for the Wertheim model is lower ($r = 0.88$).

Fig. 6 shows the dependence of a_o^N on ε_r for the TEMPAMINE and PYCM spin labels [44]. Only data for aprotic solvents are included, which again range in dielectric constant from hexane to dimethyl sulphoxide. In addition, certain apolar solvents (benzene and dioxane) and others that are not covered in Fig. 5 (dichloroethane and nitromethane) are also excluded. As in Fig. 5, the data are best fit by the Block–Walker model ($r = 0.92$ for both TEMPAMINE and PYCM). Values of the fitting constants for this model are given in Table 1. Note that the parameters derived from DTBN [44], with the same range of solvents as for TEMPAMINE and PYCM in Fig. 6, are in good agreement with those determined for DTBN from the data in Fig. 5.

Fig. 7 gives the isotropic hyperfine couplings, a_o^N, for the TEMPOL, TMA-TEMPO, PYCM and PYCA spin labels in a more limited series of aprotic solvents, ranging from tetrahydrofuran ($\varepsilon_r = 7.6$) to dimethyl sulfoxide ($\varepsilon_r = 48.2$) [27]. Previously, it was found that this series

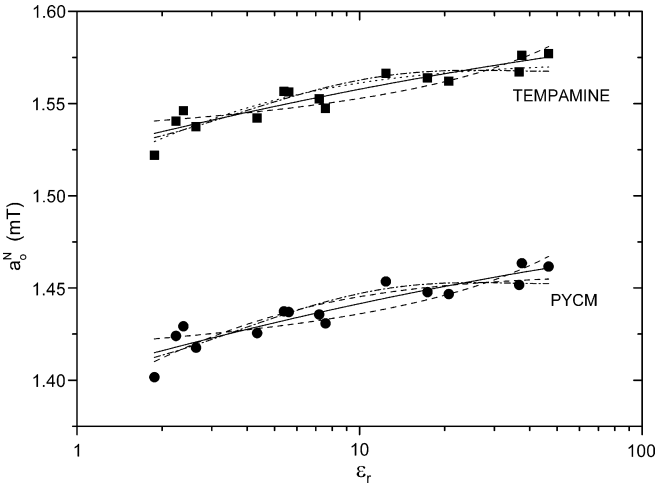

Fig. 6. Dependence of the isotropic hyperfine coupling, a_o^N, on relative dielectric permittivity, ε_r, of the solvent, for TEMPAMINE (squares) and PYCM (circles) nitroxyl spin labels. Data from Knauer and Napier [44]. Continuous lines are non-linear least-squares fits to the models specified in the caption to Fig. 5. The abscissa is logarithmic.

Table 1
Parameters fitting the dependence of a_o^N on solvent polarity according to Eqs. (5) and (14) with $f_{BW}(\varepsilon_r) = 3\varepsilon_r\ln\varepsilon_r/(\varepsilon_r\ln\varepsilon_r - \varepsilon_r + 1) - 6/\ln\varepsilon_r - 2$ (see Figs. 5–7)

Spin label	$K_v \times 10^2$ (mT)	$a_o^{\varepsilon=1}$ (mT)
DTBN	10.5 ± 1.1[a]	1.514 ± 0.004[a]
	10.3 ± 1.1[b]	1.514 ± 0.004[b]
12-SASL	10.1 ± 1.2	1.407 ± 0.004
TEMPAMINE	9.8 ± 1.1	1.524 ± 0.004
TEMPOL	9.9 ± 1.3	1.519 ± 0.006
TMA-TEMPO	9.6 ± 1.3	1.513 ± 0.006
PYCM	10.9 ± 1.3[c]	1.404 ± 0.004[c]
	9.9 ± 1.4[d]	1.410 ± 0.006[d]
PYCA	15.4 ± 2.1	1.400 ± 0.009

[a] From data of Fig. 5 [3].
[b] From data of Knauer and Napier [44] with range of solvents given in Fig. 6.
[c] From data of Fig. 6 [44].
[d] From data of Fig. 7, for more limited range of solvents [27].

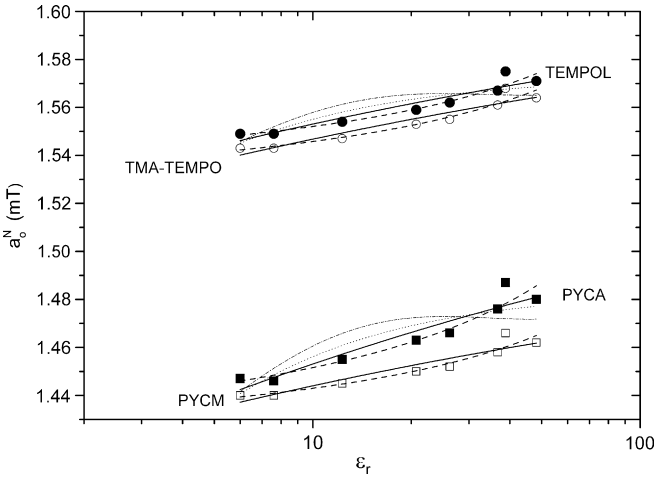

Fig. 7. Dependence of the isotropic hyperfine coupling, a_o^N, on relative dielectric permittivity, ε_r, of the solvent, for TEMPOL, TMA-TEMPO, PYCM and PYCA nitroxyl spin labels. Data from Ottaviani et al. [27]. Continuous lines are non-linear least-squares fits to the models specified in the caption to Fig. 5. The abscissa is logarithmic.

conformed to the Wertheim MSA reaction field, but without renormalisation to account for polarisability of the nitroxide [27]. This still holds after renormalisation, for this limited range of solvents (see Fig. 6); regression coefficients are $r = 0.96$–0.97. Nevertheless, reasonable fits are also obtained with the exponential-inverse model of Block and Walker ($r = 0.94$–0.95), whereas the Onsager and direct exponential models obviously describe the data less well. Fitting constants for the Block and Walker model are included in Table 1. It will be noted that the values for PYCM agree with those that were obtained from the data in Fig. 6 for this nitroxide in a wider range of solvents and for which the Block and Walker model gave the best fit.

The g-factor, as with the hyperfine coupling, also responds linearly to electric fields [45,46]. Correspondingly, the dependence of the isotropic g-value, g_o, on solvent dielectric permittivity can be described by an analogous expression:

$$g_o = g_o^{\varepsilon=1} + K_{v,g}\frac{f(\varepsilon_r)}{1-\frac{1}{4}f(\varepsilon_r)} \tag{15}$$

—cf. Eq. (14) and Ref. [29]. Fig. 8 gives the dependence of the isotropic g-value on dielectric permittivity of the solvent for the DTBN [3] and 12-SASL [29] spin labels. The best fit ($r = 0.86$) of Eq. (15) to the data for DTBN is given by the model with exponential-inverse radial dependence of ε_r [21]. For 12-SASL, however, the data is better described by the Wertheim MSA model [23,24] ($r = 0.91$). The Block and Walker model [21] gives the second-best fit ($r = 0.77$) for the isotropic g-values of 12-SASL. On the whole, however, the data for the g-values exhibit a considerably larger scatter than do those for the hyperfine couplings (compare Figs. 5 and 8).

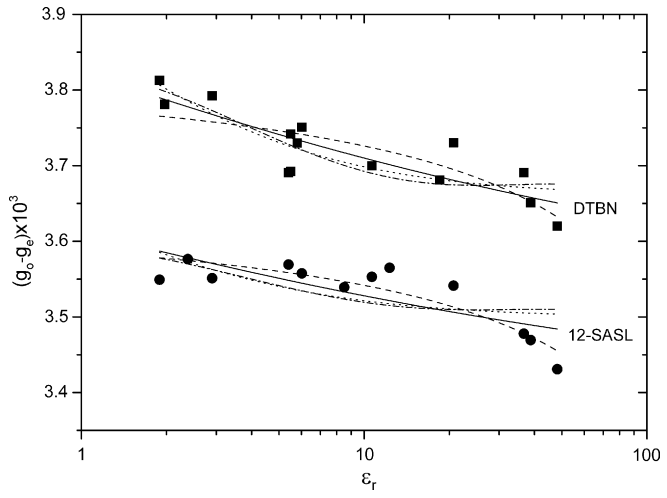

Fig. 8. Dependence of the isotropic g-value, g_o, on relative dielectric permittivity, ε_r, of the solvent, for DTBN ([3]; squares) and 12-SASL ([29]; circles) nitroxyl spin labels. Continuous lines are non-linear least-squares fits to the models specified in the caption to Fig. 5. The ordinate is expressed relative to the free-electron g-value, $g_e = 2.002319$. The abscissa is logarithmic.

4. Conclusions

The isotropic hyperfine couplings of nitroxide spin labels exhibit an approximately logarithmic dependence on the dielectric permittivity of aprotic solvents (see Figs. 5 and 6). This is inconsistent with the predictions of the Onsager model for a step transition in dielectric permittivity at the molecular surface (see Fig. 3). The transition with an exponential dependence of ε_r on inverse radial distance [21] produces a renormalised reaction field, $f_{BW}(\varepsilon_r)/\left(1-\frac{1}{4}f_{BW}(\varepsilon_r)\right)$, which, of the different models, most closely depends logarithmically on bulk dielectric permittivity (see Fig. 3). Therefore, in accordance with observation, it is expected that this model will best describe the dependence of a_o^N on ε_r for nitroxide spin labels. (Comparison with data for PYCM in Fig. 6 shows that the Wertheim MSA, which fits best in Fig. 7, performs less favourably when extended to lower values of ε_r.) In addition, theoretical studies on the polarity dependence of a_o^N for H_2NO in aprotic solvents are found to produce agreement with experiment, when the reaction field of Block and Walker is used in the calculations [38]. More recently, almost quantitative agreement has been found for the values of a_o^N for TEMPO-choline, 3-carboxy-PROXYL, and 4-carboxy-TEMPO in a range of aprotic solvents, by using DFT in combination with a polarisable continuum model [47,48].

The model of Ehrenson [22] for a direct exponential transition in dielectric permittivity at the molecular surface has previously only been applied to the analysis of a limited series of EPR hyperfine couplings [26]. After allowing for polarisation of the nitroxide, it does not offer an improvement, relative to the Block–Walker model [21], for fitting hyperfine couplings. Functionally it lies closest to the Onsager model (see Figs. 5–8) to which it is physically most related, but empirically does not perform overall as well as the latter.

Previous analyses employing alternative reaction fields to that of Onsager have neglected to include the renormalisation (Eqs. (3),(5)) that arises from polarisability of the nitroxide [20,25–27], although this was included in most analyses with the Onsager model [3,16,17]. This might account for part of the tendency to favour the Wertheim MSA model in previous analyses [20,27]. The reason being that the un-normalised Wertheim reaction field, $f_W(\varepsilon_r)$, (which applies only to unpolarisable spin labels, with $n_D = 1$) depends approximately linearly on $\ln\varepsilon_r$ (see Fig. 1). However, the Wertheim model is particularly sensitive to renormalisation and hence gives rise to large deviations from a logarithmic dependence (see Fig. 3), whereas the Block–Walker model, on the other hand, does not.

The scatter in the data for the g-values in Fig. 8 is greater than that for the hyperfine couplings of Fig. 5. Therefore, the dependence of g_o on ε_r is less appropriate for distinguishing between the different models for the reaction field. Nevertheless, the g-value data reasonably support the choice of the exponential-inverse Block–Walker model, particularly in the case of DTBN. This, therefore,

should be useful in analysing the polarity dependence of g-values that are measured with the increased precision of high-field EPR [49–51]. Not all deviations from the fits to a particular reaction field are attributable to experimental scatter. The correlation of g_o with a_o^N is better than the quality of the fits with dielectric constant in Fig. 8 [3,29]. This points to the presence of additional, more specific solvent interactions with the nitroxide that cannot be described by continuum dielectric models, but which affect both a_o^N and g_o similarly.

Finally, it should be noted that considerations similar to the above are likely to apply to the polarity dependence of chemical shifts in NMR. These too are determined by the strength of the reaction field from the dielectric environment (see, e.g., Ref. [1]).

References

[1] J.-L.M. Abboud, R.W. Taft, An interpretation of a general scale of solvent polarities. A simplified reaction field theory modification, J. Phys. Chem. 83 (1979) 412–419.

[2] P. Mukerjee, C. Ramachandran, R.A. Pyter, Solvent effects on the visible spectra of nitroxides and relation to nitrogen hyperfine splitting constants. Nonempirical polarity scales for aprotic and hydroxylic solvents, J. Phys. Chem. 86 (1982) 3189–3197.

[3] O.H. Griffith, P.J. Dehlinger, S.P. Van, Shape of the hydrophobic barrier of phospholipid bilayers. Evidence for water penetration in biological membranes, J. Membrane Biol. 15 (1974) 159–192.

[4] D. Marsh, Electron spin resonance: spin labels, in: E. Grell (Ed.), Membrane Spectroscopy. Molecular Biology, Biochemistry and Biophysics, Springer-Verlag, Berlin, Heidelberg, New York, 1981, pp. 51–142.

[5] R. Improta, V. Barone, Interplay of electronic, environmental, and vibrational effects in determining the hyperfine coupling constants of organic free radicals, Chem. Rev. 104 (2004) 1231–1253.

[6] P. Fretten, S.J. Morris, A. Watts, D. Marsh, Lipid–lipid and lipid–protein interactions in chromaffin granule membranes, Biochim. Biophys. Acta 598 (1980) 247–259.

[7] R.D. Pates, D. Marsh, Lipid mobility and order in bovine rod outer segment disk membranes. A spin-label study of lipid–protein interactions, Biochemistry 26 (1987) 29–39.

[8] R. Bartucci, A. Gambacorta, A. Gliozzi, D. Marsh, L. Sportelli, Bipolar tetraether lipids: chain flexibility and membrane polarity gradients from spin-label electron spin resonance, Biochemistry 44 (2005) 15017–15023.

[9] M. Esmann, A. Watts, D. Marsh, Spin-label studies of lipid–protein interactions in (Na^+,K^+)-ATPase membranes from rectal glands of *Squalus acanthias*, Biochemistry 24 (1985) 1386–1393.

[10] M. Esmann, D. Marsh, Spin-label studies on the origin of the specificity of lipid–protein interactions in Na^+,K^+-ATPase membranes from *Squalus acanthias*, Biochemistry 24 (1985) 3572–3578.

[11] G. Schwarzmann, P. Hoffmann-Bleihauer, J. Schubert, K. Sandhoff, D. Marsh, Incorporation of ganglioside analogues into fibroblast cell membranes. A spin-label study, Biochemistry 22 (1983) 5041–5048.

[12] M. Esmann, D. Marsh, G. Schwarzmann, K. Sandhoff, Ganglioside-protein interactions: spin-label electron spin resonance studies with (Na^+,K^+)-ATPase membranes, Biochemistry 27 (1988) 2398–2403.

[13] D. Marsh, M. Jost, C. Peggion, C. Toniolo, TOAC spin labels in the backbone of alamethicin: EPR studies in lipid membranes, Biophys. J. 92 (2007) 473–481.

[14] H.J. Steinhoff, M. Pfeiffer, T. Rink, O. Burlon, M. Kurz, J. Riesle, E. Heuberger, K. Gerwert, D. Oesterhelt, Azide reduces the hydrophobic barrier of the bacteriorhodopsin proton channel, Biophys. J. 76 (1999) 2702–2710.

[15] L. Onsager, Electric moments of molecules in liquids, J. Am. Chem. Soc. 58 (1936) 1486–1493.

[16] A.V. Gagua, G.G. Malenkov, V.P. Timofeev, Hydrogen-bond contribution to isotropic hyperfine splitting constant of a nitroxide free-radical, Chem. Phys. Lett. 56 (1978) 470–473.

[17] I. Al-Bala'a, R.D. Bates Jr., Medium effects on ESR spectra in studies of hydrogen-bonded transient solvent–solute complexes, J. Magn. Reson. 73 (1987) 78–89.

[18] D. Marsh, Polarity contributions to hyperfine splittings of hydrogen-bonded nitroxides—the microenvironment of spin labels, J. Magn. Reson. 157 (2002) 114–118.

[19] D. Marsh, Membrane water-penetration profiles from spin labels, Eur. Biophys. J. 31 (2002) 559–562.

[20] A.H. Reddoch, S. Konishi, The solvent effect on di-*tert*-butyl nitroxide. A dipole–dipole model for polar solutes in polar solvents, J. Chem. Phys. 70 (1979) 2121–2130.

[21] H. Block, S.M. Walker, Modification of Onsager theory for a dielectric, Chem. Phys. Lett. 19 (1973) 363–364.

[22] S. Ehrenson, Cavity boundary effects within the Onsager theory for dielectrics, J. Comput. Chem. 2 (1981) 41–52.

[23] M.S. Wertheim, Dielectric constant of non-polar fluids, Mol. Phys. 25 (1973) 211–223.

[24] M.S. Wertheim, Theory of polar fluids. I, Mol. Phys. 26 (1973) 1425–1444.

[25] T. Abe, S. Tero-Kubota, Y. Ikegami, Theory of solvent effects on the hyperfine splitting constants in ESR spectra of free radicals, J. Phys. Chem. 86 (1982) 1358–1365.

[26] S. Ehrenson, Classical electrical contributions to solvent polarity scales, J. Am. Chem. Soc. 103 (1981) 6036–6043.

[27] M.F. Ottaviani, G. Martini, L. Nuti, Nitrogen hyperfine splitting constant of nitroxide solutions: differently structured and charged nitroxides as probes of environmental properties, Magn. Reson. Chem. 25 (1987) 897–904.

[28] D. Marsh, M. Jost, C. Peggion, C. Toniolo, Lipid chainlength dependence for incorporation of alamethicin in membranes: EPR studies on TOAC-spin labelled analogues, Biophys. J. 92 (2007) 4002–4011.

[29] D. Marsh, C. Toniolo, Polarity dependence of EPR parameters for TOAC and MTSSL spin labels: correlation with DOXYL spin labels for membrane studies, J. Magn. Reson. (2007), accepted for publication.

[30] Y.V.S. Rama Krishna, D. Marsh, Spin label ESR and ^{31}P-NMR studies of the cubic and inverted hexagonal phases of dimyristoylphosphatidylcholine/myristic acid (1:2, mol/mol) mixtures, Biochim. Biophys. Acta 1024 (1990) 89–94.

[31] K. Schorn, D. Marsh, Lipid chain dynamics and molecular location of diacylglycerol in hydrated binary mixtures with phosphatidylcholine: spin label ESR studies, Biochemistry 35 (1996) 3831–3836.

[32] D. Marsh, Polarity and permeation profiles in lipid membranes, Proc. Natl. Acad. Sci. USA 98 (2001) 7777–7782.

[33] T. Páli, M.E. Finbow, D. Marsh, Membrane assembly of the 16-kDa proteolipid channel from *Nephrops norvegicus* studied by relaxation enhancements in spin-label ESR, Biochemistry 38 (1999) 14311–14319.

[34] W.L. Hubbell, A. Gross, R. Langen, M.A. Lietzow, Recent advances in site-directed spin labeling of proteins, Curr. Opin. Struct. Biol. 8 (1998) 649–656.

[35] W.L. Hubbell, D.S. Cafiso, C. Altenbach, Identifying conformational changes with site-directed spin labeling, Nat. Struct. Biol. 7 (2000) 735–739.

[36] Y. Murata, N. Mataga, ESR and optical studies on the EDA complexes of di-*t*-butyl-*N*-oxide radical, Bull. Chem. Soc. Japan 44 (1971) 354–360.

[37] A.M. Vasserman, A.L. Buchachenko, E.G. Rozantsev, M.B. Neiman, Dipole moments of molecules and radicals di-*tert*-butyl nitrogen oxide, J. Struct. Chem. 6 (1966) 445–446.

[38] V. Barone, Electronic, vibrational and environmental effects on the hyperfine coupling constants of nitroside radicals. H_2NO as case study, Chem. Phys. Lett. 262 (1996) 201–206.

[39] D.E. Sullivan, J.M. Deutch, Local field models for light scattering and the dielectric constant of nonpolar fluids, J. Chem. Phys. 64 (1976) 3870–3878.
[40] D.E. Sullivan, J.M. Deutch, Dielectric models for solvent effects on electronic spectra, J. Chem. Phys. 65 (1976) 5315–5317.
[41] A.H. Cohen, B.M. Hoffman, Acceptor strengths of some group IV Lewis acids by electron paramagnetic resonance studies of their complexes with aliphatic nitroxides, Inorgan. Chem. 13 (1974) 1484–1491.
[42] R.N. Schwartz, M. Peric, S.A. Smith, B.L. Bales, Simple test of the effect of an electric field on the ^{14}N-hyperfine coupling constant in nitroxide spin probes, J. Phys. Chem. B 101 (1997) 8735–8739.
[43] J.G. Kirkwood, The dielectric polarization of polar liquids, J. Chem. Phys. 7 (1939) 911–919.
[44] B.R. Knauer, J.J. Napier, Nitrogen hyperfine splitting constant of nitroxide functional group as a solvent polarity parameter - relative importance for a solvent polarity parameter of its being a cybotactic probe vs its being a model process, J. Am. Chem. Soc. 98 (1976) 4395–4400.
[45] A.F. Gullá, D.E. Budil, Orientation dependence of electric field effects on the *g* factor of nitroxides measured by 220 GHz EPR, J. Phys. Chem. B 105 (2001) 8056–8063.
[46] M. Plato, H.J. Steinhoff, C. Wegener, J.T. Törring, A. Savitsky, K. Möbius, Molecular orbital study of polarity and hydrogen bonding effects on the *g* and hyperfine tensors of site directed NO spin labelled bacteriorhodopsin, Mol. Phys. 100 (2002) 3711–3721.
[47] A.M. Tedeschi, G. D'Errico, E. Busi, R. Basosi, V. Barone, Micellar aggregation of sulfonate surfactants studied by electron paramagnetic resonance of a cationic nitroxide: an experimental and computational approach, Phys. Chem. Chem. Phys. 4 (2002) 2180–2188.
[48] G.A.A. Saracino, A.M. Tedeschi, G. D'Errico, R. Improta, L. Franco, M. Ruzzi, C. Corvaia, V. Barone, Solvent polarity and pH effects on the magnetic properties of ionizable nitroxide radicals: a combined computational and experimental study of 2,2,5,5-tetramethyl-3-carboxypyrrolidine and 2,2,6,6-tetramethyl-4-carboxypiperidine nitroxides, J. Phys. Chem. 106 (2002) 10700–10706.
[49] D. Marsh, D. Kurad, V.A. Livshits, High-field electron spin resonance of spin labels in membranes, Chem. Phys. Lipids 116 (2002) 93–114.
[50] D. Kurad, G. Jeschke, D. Marsh, Lipid membrane polarity profiles by high-field EPR, Biophys. J. 85 (2003) 1025–1033.
[51] V.A. Livshits, D. Kurad, D. Marsh, Simulation studies on high-field EPR of lipid spin labels in cholesterol-containing membranes, J. Phys. Chem. B 108 (2004) 9403–9411.